MJFAS MALAYSIAN JOURNAL OF FUNDAMENTAL AND APPLIED SCIENCES
PRINT ISSN: 2289-5981 | ONLINE ISSN: 2289-599X

RESEARCH ARTICLE

Structural analysis and luminescence studies of Eu^{3+} doped magnesium borophosphate ceramic

Siti Maisarah Aziz [a,*], Roslan Umar [b], Nurulhuda Binti Mohammad Yusoff [a], Salmiah Jamal Mat Rosid [a], Siti Noor Syuhada Mohd @ Muhammad Amin [a]

[a] *UniSZA Science and Medicine Foundation Centre, Universiti Sultan Zainal Abidin, Gong Badak Campus, 21300 Kuala Nerus, Terengganu, Malaysia*
[b] *East Coast Environmental Research Institute (ESERI), Universiti Sultan Zainal Abidin, Gong Badak Campus, 21300, Gong Badak, Kuala Nerus, Terengganu*

** Corresponding author: smaisarahaziz@unisza.edu.my*

Article history
Received 4 May 2020
Revised 10 June 2020
Accepted 5 August 2020
Published Online 20 October 2020

Abstract

The structural and optical properties of Europium (Eu^{3+}) ions doped magnesium borophosphate (MBP) ceramic synthesized via solid state reaction method have been studied. The influences of varying Eu_2O_3 concentrations on structural and optical properties have been determined. X-ray Diffraction (XRD) pattern revealed that the prepared MBP ceramic existed in polycrystalline phase of $B(PO_4)$, $Mg(PO_3)_2$ and $Mg_3(BO_3)(PO_4)$. FTIR spectra displayed the presence of P-O stretching modes of P-O-P, P=O and PO_4 unit, BO_3 and BO_4 bridging oxygen. The emission peaks of Eu^{3+} doped sample were located at 593 nm, 613 nm, 657 nm and 700 nm due to the transitions of $^5D_0$- ^7F_J (J = 1,2,3 and 4). The 1.5 mol % of Eu^{3+} doped MBP ceramic showed an intense luminescence with a very sharp peak dominated by the $^5D_0$-$^7F_1$ transition at 593 nm.

Keywords: luminescence, rare-earths, borophosphate, ceramic, europium

INTRODUCTION

Ceramics have been extensively investigated because it is crucial in the development of laser and solid-state lighting. New ceramic materials have been developed for advanced ceramic engineering applications especially in semiconductors (Daqin *et al.,* 2017). To date, ceramic plays an important role in the human economy and everyday life, such as in optical devices and electronics due to its high temperature resistance, high hardness, corrosion resistance, and electrical conductivity (Chen *et al.,* 2015). Ceramics are not only known for their excellent thermal and mechanical properties, they also have the potential to become good luminescence material due to its opaque characteristic which enhances the absorption efficiency of rare earth ions (Xu *et al.,* 2015). This excellent property makes them further usable in optimizing luminescent material.

Phosphate (P_2O_5) exhibits lot of advantages as host material compared to borate and silicate due to its easy preparation in various composition, high thermal expansion coefficient, low melting temperature, high ultra violet (UV), and far infrared transmissions (Liu *et al.,* 2015). However, this material also has some disadvantages such as poor chemical durability, high hygroscopic, and volatile nature of phosphate which limit them from replacing conventional ceramics in technology applications (Xiaobin *et al.,* 2019). To overcome this, an addition of borate into the phosphate host will alter the structural unit of the network (Areej *et al.,* 2020). The incorporation of metal oxide is necessary due to confinement of phosphate in chemical durability in order to stabilize the ceramic structure. According to a previous study, comparing to pure borate and pure phosphate alone, the combination of phosphate and borate is rather an intrinsically interesting subject of study due to the stability of borophosphate (BP) compound (Mengjie *et al.,* 2019, Leong *et al.,* 2015).

The basic units of borate are trigonal BO_3 groups while the phosphate is PO_4 tetrahedra that linked through the covalent bridging oxygens. Fei *et al.* stated that BP is drawing a tremendous attention due to the combination of the two network formers borate and phosphate which are motivated by replacing P-O-P bonds to P-O-B bonds in the ceramic structure. Metal oxides such as MgO are found to be good stabilizers due to MgO can act as modifier which able to change the structural features of the ceramic network (Chye *et al.,* 2017). MgO as a modifier imparts better chemical durability and have a strong influence on the structural properties. This oxide entered the network in two forms either as modifier or as both modifier and former. Recently, rare earth ions (REIs) doped ceramic received large attention due to its diverse applications. Some of the applications include medical equipment, solid state laser and visible display devices (Sen *et al.,* 2019). The intensity of emission is affected by the ability of the luminescence material to fully occupy an electronic excited state, as well as the ability to inhibit its non-radiative decay (Libin *et al.,* 2018). It is well known that Eu^{3+} is one of the most important activators for many different host lattices because of its rich red emission where are widely used in field emission technology and LEDs (Xiangyu *et al.,* 2017). Previous research reported that $LaAlGe_2O_7$ doped Eu^{3+} has been identified as another good material which displayed an intense red emission under ultraviolet (UV) sources (Chun Li *et al.,* 2010). Besides, $LaAlGe_2O_7$ doped Eu^{3+} ions

show good luminescence properties in variety of lattices. Thus, $LaAlGe_2O_7$ doped Eu^{3+} is a potential red-emitting phosphor due to excellent luminescent properties and is used as novel optical materials. Up until now, REIs doped luminescence material has become an interesting topic in luminescence area. In order to pursue this area, a new ceramic composition was developed and presented. The influences of Eu^{3+} in polycrystalline structural system of magnesium borophosphate (MBP) ceramic are still remained and its detailed analysis about this impact has not been established yet. Moreover, doubtfulness of the influence activator concentrations of Eu^{3+} onto host network modified luminescence properties should be clarified in this study. A detailed study on Eu^{3+} doped MBP ceramics was carried out and the result was analyzed and presented.

MATERIALS AND METHODS

Raw materials i.e. phosphoric acid (H_3PO_4), orthoboric acid (H_3BO_3, Sigma Aldrich 99.9%), magnesium oxide (MgO, Sigma Aldrich 99.9%), and Europium (III) oxide (Eu_2O_3, Sigma Aldrich 99.9%) were weighed and mixed according to the compositions, respectively. These mixtures were stirred using a magnetic stirrer at 80 °C for 2 hours to ensure the homogeneity of the samples before being placed into an alumina crucible. These samples were calcined at 900 °C for 5 hours in the furnace. After that, all samples were grounded into powder for structural and luminescence analysis. The crystallization phases were identified using X-ray Diffractometer (Siemens Diffractometer D5000) system operating at 40 kV, 30 mA in the 2θ range from 10 ° to 90 °. FTIR spectroscopy was used to identify the functional group bonding vibrational modes. A 2 mg of powder sample was mixed with potassium bromide in the ratio of 1:100 before pressed into pellet form with thickness of 1.0 mm and 2 cm diameter under pressure of 5 ton per square inch. The FTIR Spectra in the 400–4000 cm^{-1} range were recorded by Perkin-Elmer Spectrum one FT-Infrared Spectrum with 100-step scanning at 4 cm^{-1} resolution. Emission spectrum and lifetime measurement of samples were analyzed using Jasco Photoluminescence Spectroscopy. The sample is placed in the sample holder and scanned with xenon lamp as a source of excitation for emission spectrum wavelengths in the visible range from 200 nm to 900 nm. The nominal compositions and the codes of synthesized ceramic were listed in Table 1.

Table 1 Sample codes and their nominal compositions (mol %).

Sample code	B_2O_3	P_2O_5	MgO	Eu_2O_3
MBP:Eu0.5	59.5	15.0	25.0	0.5
MBP:Eu1.0	59.0	15.0	25.0	1.0
MBP:Eu1.5	58.5	15.0	25.0	1.5
MBP:Eu2.0	58.0	15.0	25.0	2.0

RESULTS AND DISCUSSIONS

X-ray diffraction analysis

XRD pattern is one of the most convenient and common method to determine the phase of sample. Fig. 1 presents the XRD pattern of MBP ceramic.

Fig. 1 displays the XRD pattern which consisted of sharp peaks indicating the prepared samples are confirmed in polycrystalline phases such as B(PO4), Mg(BO3)(PO4), and Mg(PO3)2. These strong and narrow peaks clearly indicated that the prepared samples are of good crystalline order. The pattern exemplified the Mg(BO3)(PO4) peak is in good agreement with standard JCPDS card number (00-053-0778) and becoming predominant phase followed by monoclinic crystal of Mg(PO3)2 (00-027-1273) and tetragonal crystal of B(PO4) (01-072-9921) phase. Interestingly, doping of Eu3+ shows no additional peak which confirmed none additional impurity phases formation and due to its small concentration in samples. This XRD pattern exhibits that the europium ion has been uniformly dispersed into the structure network of MBP ceramic as reported elsewhere (Shi et al., 2013).

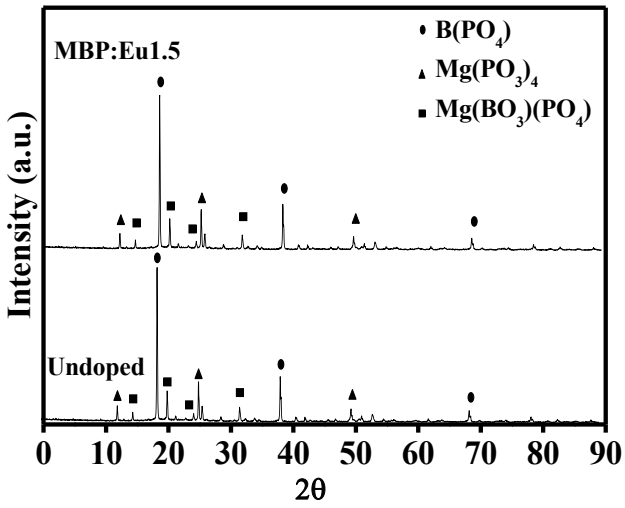

Fig. 1 XRD pattern of MBP:Eu1.5 and undoped sample as reference.

Infrared spectra

The structural features of corresponding magnesium borophosphate ceramic were measured by means of FT-Infrared Spectroscopy. The main goal of infrared spectroscopy analysis is to determine the functional group in the sample. The discussion will be on the absorption spectra obtained in the frequency ranging from 400 to 4000 cm^{-1} for all samples. The infrared spectra in Fig. 2 clearly comprised of main sharp distinctive and characteristic absorption bands of prepared samples. These bands are due to main borophosphate network group vibration. Table 2 summarized infrared peak positions and bonding vibration assignments. The vibrations of the borate network appeared in the range between 800-1600 cm^{-1}. The absorption band around 800-1200 cm^{-1} are assigned to BO_4 unit and the band around 1200-1600 cm^{-1} are allocated to the vibration of borate in BO_3 units. The absorption band of BO_4 is consistent for all prepared samples with various concentrations of Eu_2O_3. Meanwhile, the infrared band located around 1250 cm^{-1} is indicated to Mg-O bending vibration (Lei *et al.,* 2018). There are four main regions which can be acknowledged for phosphate. The region around 710-950 cm^{-1} is known as P-O-P terminals and the band at 1300 cm^{-1} is due to the P=O vibration in PO_4 unit. The other band at 1090 cm^{-1} is characterized as O-P-O group of non-bridging oxygen in phosphate chain. The vibration of PO_2 is identified at 1170-1200 cm^{-1}. The bands located around 1650 cm^{-1} to 1700 cm^{-1} is relatively weak and can be described as the stretching vibrations of P-O-H group (Kumar *et al.,* 2018). Further, formation of hydroxyl groups corresponded to the H-O-H and OH group are appeared in the range of 1600 cm^{-1} to 1700 cm^{-1} and 32 00 cm^{-1} to 3400 cm^{-1}, respectively. The infrared spectrum exhibits two broad bands in the range of 1900 to 4000 cm^{-1} which showed the characteristic of H_2O bands.

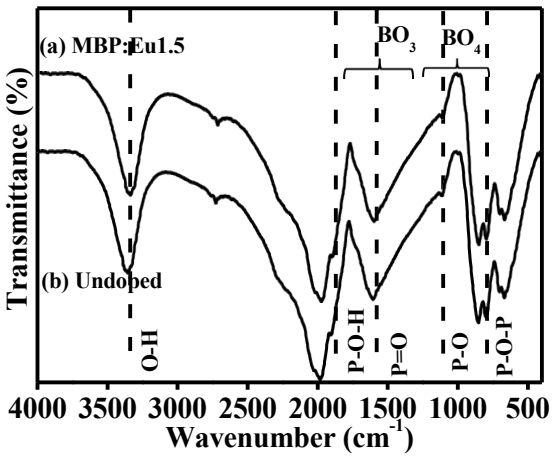

Fig. 2 Infrared spectra of (a) MBP:Eu1.5 ceramic and (b) Undoped sample for comparison.

From Fig. 2, the bands at 3220 cm^{-1} and 3445 cm^{-1} can be attributed to the symmetric stretching vibration of (O-H) and (H-O-H) which is related to vibration of water and hydroxyl group in the sample. In particular, the atmospheric moisture is easily absorbed by the sample powder causing the appearance of infrared band belonging to H_2O molecules although the sample under investigation does not contain H_2O as unit in the network. The occurrence of these bands is probably due to water absorptions during the pallet preparation with KBr. It is clear from Fig. 2, the addition of the Eu^{3+} in the magnesium borophosphate ceramic did not show any permanent changes to the infrared spectra. This result is consistent with the previous report that implies no additional peaks were observed in infrared absorption bands (Wang *et al.,* 2017).

Tables 2 Infrared bands assignments of the present magnesium borophosphate ceramic.

Band Center (cm^{-1})	Assignments
600-800	B-O stretching vibrations in borate groups
846-860	Attributed to PO_2 stretching of the doubly bonded oxygen vibrations (P=O)
905	Asymmetric stretching vibration of P-O-P groups
1285	Mg-O bending stretching
1087	Asymmetric stretching of PO_3 groups
860-1200	B-O bending vibrations in BO_4 unit
1200-1600	B-O stretching vibration in BO_3 unit
1650-1700	P-O-H stretching vibrations
1634	Different stretching modes of (OH) group
3498	Asymmetric and symmetric stretching modes of interstitial H_2O molecule

Luminescence spectra

Fig. 3 illustrates the luminescence spectra of MBP:Eu1.5 under 390 nm excitations. All peaks of Eu^{3+} are observed in the visible region spectral range of 550 to 750 nm.

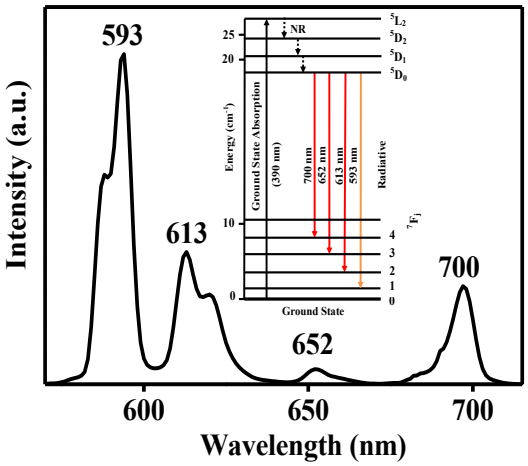

Fig. 3 Luminescence spectra of Eu^{3+} ions doped MBP:Eu1.5 ceramics [Inset shows the schematic energy level diagram for Eu^{3+} emission at 390 nm excitation].

The Eu_2O_3 concentration dependent emission spectra (Fig. 3) consist of intense emissions at 593 nm (orange), 613 nm (red), 652 nm (red), and 700 nm (red) which nominated to the transitions of $^5D_0$-^7F_J (J = 1, 2, 3, 4). These emissions intensities illustrate that the peak at 593 nm is stronger than 613 nm which means it was dominated by the $^5D_0$-$^7F_1$ transition. It is well-known that the $^5D_0$ -$^7F_1$ transition belongs to the magnetic dipole transition which scarcely changed the crystal field strength around the Eu^{3+} ions (Matas *et al.,* 2016). This signifies that Eu^{3+} occupied the inversion symmetry site in the lattice. On the other hand, the electric dipole transition ($^5D_0$-$^7F_2$) is prominent in the emission spectra and its intensity appeared very sensitive to the symmetrical site of the Eu^{3+} ions (Aziz *et al.,* 2017). Insert figure describes the energy levels for the emissions' process observed for Eu^{3+} ions doped MBP ceramic. Energy diagram shows that the absorption of Eu^{3+} ions are excited from $^7F_0$ level to higher level ($^5L_2$) with 390 nm excitation wavelength via ground state absorption (GSA). Then, the electron is expected to relax at $^5D_0$ level as the metastable level through the relaxation process before it undergoes to a stable state. The Eu^{3+} ions are partially relaxed at $^5D_2$ and $^5D_1$ levels as non-radiative (NR: $^5L_6 \rightarrow {}^5D_{2,1}$). These NR emissions is released in form of heat and disappeared due to energy loss. From $^5D_0$ level, electrons are straightly dropped to $^7F_1$, $^7F_2$, $^7F_3$ and $^7F_4$ levels' emissions. The first wavelength gives orange emission spectrum at 593 nm followed by red emission spectrum at 613 nm, 657 nm and 700 nm. All transitions of emission spectra of Eu^{3+} can be corresponded to energy level. The composition with the highest luminescence intensity is associated by the influence of various concentrations of Eu^{3+} ions. Fig. 3 displays the room temperature luminescence spectra of all MBP ceramic samples with excitation was at 390 nm. It describes the variation of intensity bands as function of Eu^{3+} concentrations within the range of 550 nm to 720 nm.

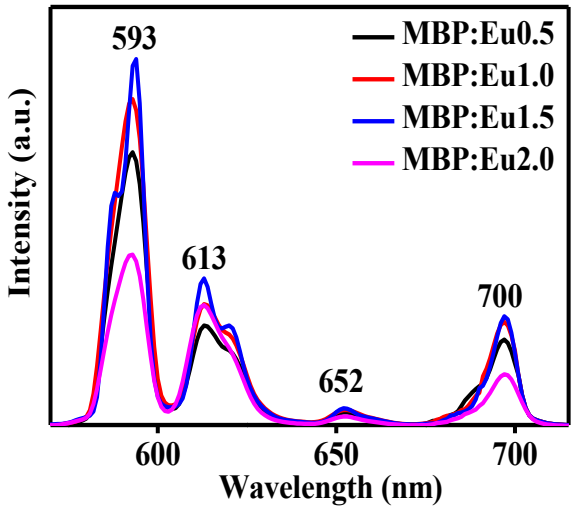

Fig. 4 Luminescence spectra of all ceramic samples with 390 nm excitation.

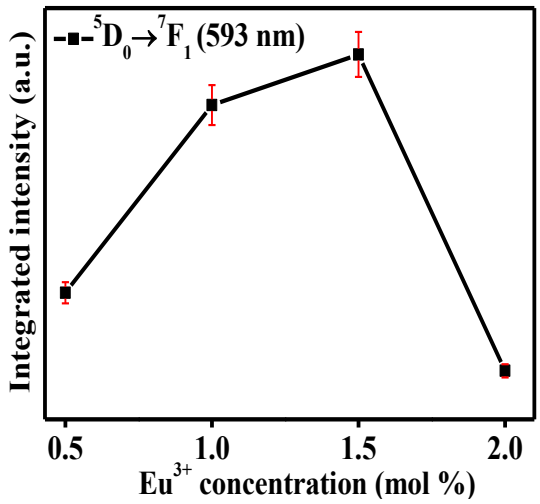

Fig. 5 Dependency of $^5D_0 \rightarrow {}^7F_1$ integrated emission intensity of MBP:Eu^{3+} on doping concentration upon 390 nm excitation.

The luminescence spectra in Fig. 4 exhibits emission bands at 593 nm, 613 nm, 652 nm, and 700 nm corresponding to $^5D_0$-^7F_J (J = 1, 2, 3 and 4) levels. It is found that the emission intensity for the transition of $^5D_0 \rightarrow {}^7F_2$ is much stronger than $^5D_0 \rightarrow {}^7F_1$. Intensity of the emission is significantly increased as the concentration of Eu_2O_3 is increased. Generally, the optimization of Eu^{3+} concentration is influenced by two main factors which is the higher concentration of doping leads to the increment of the luminescence centers number thus increasing the radiative recombination. Consequently, there is also an increase of the probability of energy transfer between europium ions, which enhanced the efficiency of the nonradiative processes (Kolesnikov *et al.,* 2017). As can be seen, first emission intensity increased with the increasing of doping concentration of Eu^{3+} ions. However further increased concentration of beyond 1.5 mol% intensity significantly reduced. This phenomenon is called the concentration quenching effects of Eu^{3+} in MBP ceramic. The quenching and enhancement constituent for each transition is evaluated and listed in Table 3.

Table 3 Eu_2O_3 concentration dependence of integrated emission intensity $^5D_0$- ^7F_J (J = 1,2,3,4).

Sample code	Eu_2O_3 (mol %)	Integrated intensity ratio (a.u.)
MBP:Eu0.5	0.5	1:1:1:1
MBP:Eu1.0	1.0	1.19:1.22:1.19:1.20
MBP:Eu1.5	1.5	1.33:1.47:1.28:1.29
MBP:Eu2.0	2.0	0.62:1.20:0.68:0.60

From the luminescence spectra, the integrated intensity of the $^5D_0 \rightarrow {}^7F_1$ transition is plotted versus Eu_2O_3 concentrations as shown in Fig. 5.

The quenching and enhancement factor for $^5D_0 \rightarrow {}^7F_1$ transition are presented in Fig. 5. The intensity is first increased from 2026 a.u. to 2708 a.u. at 1.0 mol % of Eu_2O_3 and decreased thereafter. It suggested that both multiphonon relaxation and cross-relaxation by resonant energy transfer were responsible for the reddish orange emission enhancement as described elsewhere (Das *et al.,* 2012). However, beyond 1.5 mol %, the emission intensity decreased due to the concentration quenching on the luminescence. This was attributed by the excessive doping of emission spectrum ion in inorganic materials which leads to a slight decrement in emission intensity. This result is consistent with the previous research which is called as a phenomenon of concentration quenching (Bandi *et al.,* 2012). This quenching takes place when the migration ions to excitation energy between the emission ions or the migration of energy to quenching centers thus the excitation energy was lost via a non-radiative transition (Song *et al.,* 2013). Additionally, the decrement intensity of emission may be due to alteration structural by interaction among Eu^{3+} ions in the network structure of ceramics. From the result in Fig. 4 it can be concluded that 1.5 mol % at 593 nm is the optimum concentration of Eu^{3+} which is potentially used for display materials emitting reddish orange color applications. Tables 4 and 5 enlist the estimated full width at half maximum (FWHM) and the quality factor (Q) for the prepared samples.

Table 4 Peak transitions and FHWM (nm) of prepared ceramics.

Sample code	Eu_2O_3 (mol%)	FWHM (nm)			
		$^5D_0 \rightarrow {}^7F_1$	$^5D_0 \rightarrow {}^7F_2$	$^5D_0 \rightarrow {}^7F_3$	$^5D_0 \rightarrow {}^7F_4$
MBP:Eu0.5	0.5	7.05	10.92	12.86	12.53
MBP:Eu1.0	1.0	6.98	11.19	12.97	12.15
MBP:Eu1.5	1.5	5.40	10.64	12.9	11.92
MBP:Eu2.0	2.0	6.32	11.25	12.25	12.51

Table 5 Peak transitions and quality factor (Q) of prepared ceramics.

Sample Code	Eu_2O_3 (mol%)	Quality factor, Q			
		$^5D_0 \rightarrow {}^7F_1$	$^5D_0 \rightarrow {}^7F_2$	$^5D_0 \rightarrow {}^7F_3$	$^5D_0 \rightarrow {}^7F_4$
MBP:Eu0.5	0.5	84.11	56.13	50.69	55.86
MBP:Eu1.0	1.0	84.95	54.78	50.26	57.61
MBP:Eu1.5	1.5	109.81	57.61	50.26	58.72
MBP:Eu2.0	2.0	54.48	54.48	53.22	55.95

Table 5 shows the Eu_2O_3 concentrations dependent quality factor, which is the main indicator of stimulated emission for laser active medium (Zhi *et al.,* 2019). With increasing concentrations of Eu_2O_3, the corresponding quality factor values remarkably increased. A higher value of quality factor indicated more intense laser transitions (Aziz *et al.,* 2017, Lyuchao *et al.,* 2019). The presence of Eu_2O_3 undoubtedly decreased the non-radiative energy loss.

Fig. 6 shows the decay profile of Eu^{3+} emission for $^5D_0 \rightarrow {}^7F_1$ transition recorded at room temperature by exciting with 390 nm wavelength.

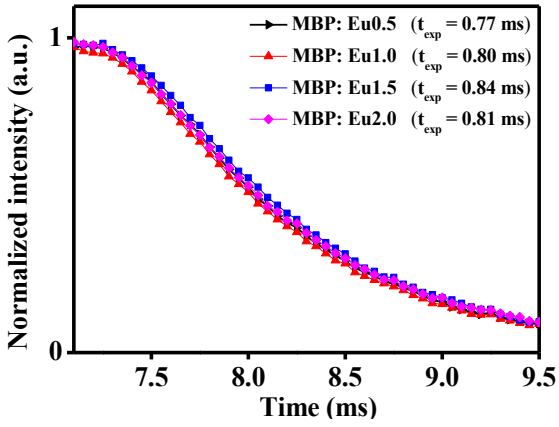

Fig. 6 Decay profile for $^5D_0 \rightarrow {}^7F_1$ emission of magnesium borophosphate ceramic under excitation 390 nm.

Fig. 6 exhibits a strong dependence lifetime of $^5D_0$ level ($^5D_0 \rightarrow {}^7F_1$, 593 nm) on concentrations of Eu_2O_3 at 390 nm excitations. The decay curves of all the prepared ceramics were found to be single exponential and enlisted in Table 6.

Table 6 Eu_2O_3 concentrations dependent τ value of $^5D_0 \rightarrow {}^7F_1$ transitions.

Sample	Eu_2O_3 (mol %)	Transition $^5D_0 \rightarrow {}^7F_1$ $\lambda_{emission}$ (nm)	τ (ms)
MBP:Eu0.5	0.5	592	0.77
MBP:Eu1.0	1.0	592	0.80
MBP:Eu1.5	1.5	593	0.84
MBP:Eu2.0	2.0	593	0.81

The excited state lifetime of each sample was calculated via,

$$I_t = I_0 \, e^{-t/\tau} \quad (1)$$

where I_t and I_0 are the luminescence intensities at time t = 0 and at 't' respectively, τ is the lifetime of the excited level (Aziz *et al.,* 2018). In the present study, the calculated values of experimental lifetime (τ) for the MBP:Eu0.5, MBP:Eu1.0, MBP:Eu1.5 and MBP:Eu2.0 samples were 0.77, 0.80, 0.84 and 0.81 ms, respectively. The range of lifetime of the samples in a good agrees with the previous reports on decay analysis of europium ions (Meng *et al.,* 2015). It is well known that this attributed of conjunction of rare earth clustering with energy transfers between clustered ions by a cross-relaxation mechanism or phonon-assisted energy transfer. As a result, at higher concentrations of Eu_2O_3 the lifetime of emission dramatically drops due to the formation of exchange coupled Eu pairs (Qolyeva *et al.,* 2019). The reduction of the sample lifetime at room temperature ascribed to thermal quenching. The lifetime of MBP:Eu1.5 ceramic is slightly longer compared to other ceramic samples which further indicates that rare earth ions were successfully embedded in the crystal phase and prove the low phonon energy environment of Eu^{3+} ions in the ceramic. Luminescence lifetimes for excited states of rare earth ions usually increase due to higher multiphonon relaxation rates and lower radiative quantum efficiencies (Qui *et al.,* 2017). Therefore, it is in agreement with luminescence emission spectra intensity where stronger-luminescence intensity shows slower decays emission.

CONCLUSION

The influence of Eu_2O_3 incorporated on the structural and optical properties of MBP ceramic system were established. Ceramic samples was prepared via solid state method and thoroughly characterized. XRD pattern affirmed the polycrystalline phases of prepared ceramics. FTIR spectra revealed the presence structural units of phosphate and borate in ceramic network irrespective of Eu_2O_3 concentrations. The observed luminescence enhancement and quenching was ascribed to the interaction among europium ions. Among the studied ceramics, MBP:Eu1.5 ceramic displayed the highest intensity corresponding to the $^5D_0 \rightarrow {}^7F_1$ transition at 593 nm. Results suggested that these ceramics can be promising for development of solid-state lasers application.

ACKNOWLEDGEMENT

The authors would like to thank UTM for the financial support provided through the Vot. 4F424 for this project.

REFERENCES

Areej S, Hussin R., Alamri, S. N. Ghoshal, S. K. (2020). Spectral features of Ho^{3+} -doped boro-phosphate glass-ceramics: Role of Ag nanoparticles sensitization. *Journal of Luminescence*, 223, 117-128.

Aziz, S. M, Hussin R., Yusoff. N. M. (2015). Structural and Luminescence Properties of Eu^{3+} and Dy^{3+} Doped Magnesium Tellurite Borophosphate Ceramic. *Advanced Materials Research*, 1107,53-58.

Aziz, S. M, Sahar, M. R, Ghoshal, S. K. (2018). Spectral attributes of Eu^{3+} doped borotellurite glasses containing Mn_3O_4 nanoparticles. *Journal of Alloys and Compounds*, 735,1119-1130.

Aziz, S. M. Sahar, M. R. Ghoshal S. K. (2017). Modified magnetic and optical properties of manganese nanoparticles incorporated europium doped magnesium borotellurite glass. *Journal of Magnetism and Magnetic Materials*, 423, 98-105

Bandi, V. R. Grandhe, B. K. Woo, H. Jang, Shin, K. D. Yi, S. Jeong, J. (2012). Luminescence and energy transfer of Eu^{3+} or/and Dy^{3+} co-doped in Sr_3AlO_4Fphosphors with NUV excitation for WLEDs. *Journal Alloy and Compounds*, 538, 85-90.

Chen, D. Q, Xiang W. D., Liang X. J. (2015). Advances in transparent glass-ceramic phosphors for white light-emitting diodes-a review. Journal of the European Ceramic Society, 35, 859–869.

Chye M. Y. (2017). *Crystalline phase and spectroscopic properties of copper-containing borophosphate ceramic doped with samarium oxide*. Universiti Teknologi Malaysia.

Daqin, C., Shen L., Xinyue L., Shuo Y., Ping H .(2017).Upconverting luminescence based dual-modal temperature sensing for $Yb^{3+}/Er^{3+}/Tm^{3+}$: YF_3 nanocrystals embedded glass ceramic. Journal of the European Ceramic Society, 37, 15, 4939-4945.

Das, S., Amarnath Reddy, A. and Vijaya Prakash, G. (2012). Near white light emission from K^+ ion compensated $CaSO_4:Dy^{3+}Eu^{3+}$ phosphors. *Ceramics International*, 38, 5769-5773.

Fei, S., Yong, C., Jiwen, X. T., Yang, Y., Guohua, C. (2019). Up-conversion luminescence and highly sensing characteristics of Er^{3+}/Yb^{3+} co-doped borophosphate glass-ceramics. *Optics Communications*, 441, 38-44.

Golyeva, E. V. Vaishlia, E. I. Chernovets, B. V, Kolesnikov. I. E. (2019). Luminescent properties of $YVO_4:Eu^{3+}$ ceramic phosphors according to Li^+ content. *Materials Today Proceeding*, 75, 15-20.

Huitao, Z., Ning G., Qimeng L., Yu D., Ying P., Yueyue S., Ruizhuo O., Yuqing M., Baiqi S. (2019). Novel ratiometric optical thermometry based on dual luminescent centers from europium doped $LiCa_3MgV_3O_{12}$ phosphor. Ceramics International, 45, 16651-16657.

Kazuki, A., Jumpei, U., Setsuhisa, T. (2019). Long persistent luminescence and blue photochromism in Eu^{2+}-Dy^{3+} co-doped barium silicate glass ceramic phosphor. *Journal of Luminescence*, 207, 246-250.

Kolesnikov, I. E. Mamonova, D. V. Lähderanta, E. Kurochkin, A. V. Mikhailov, M. D. (2017). The impact of doping concentration on structure and photoluminescence of Lu_2O_3 :Eu $^{3+}$ nanocrystals. *Journal of Luminescence*, 187, 26-32.

Kumar, R. Singh. H. S. Singh, Y. (2018). FTIR characterization of $Bi_2Sr_2Ca_{n-1}(Cu_{1-x}Fe_x)_3O_{10+\delta}$ with (n=3, x = 0.01) ceramic superconductor. *AIP Conference Proceedings,* 1953, 30-35.

Lei, H. Zhang, Q. Luo, Z. (2018). Crystallization, structure and characterization of MgO-Al_2O_3-SiO_2-P_2O_5 transparent glass-ceramics with high crystallinity. *Journal of Non-Crystalline Solids*, 481(2018) 123–131.

Leong P. M. (2015). Structural and luminescence properties of europium oxide and dysprosium oxide codoped strontium borophosphate ceramics. *Universiti Teknologi Malaysia.*

Li, Chun. Yen, H. Yu, F. (2010). Synthesis and luminescent properties of Ln^{3+} (Eu^{3+}, Sm^{3+}, Dy^{3+})-doped lanthanum aluminum germanate $LaAlGe_2O_7$ phosphors. *Journal of Alloys and Compounds*, 439,367-375

Libin, X., Qinghui, X., Xinyu Y., Weixiong Y., Tongxiang, L. (2018). Erosion behavior and luminescence properties of $Y_3Al_5O_{12}:Ce^{3+}$-embedded calcium bismuth borate glass-ceramics for WLEDs. *The American Ceramic Society*, 4, 2053-2065.

Liu, X. Chen, G. Chen, Y. Yang, T. (2017). Luminescent characteristics of $Tm^{3+}/Tb^{3+}/Eu^{3+}$ tri-doped phosphate transparent glass ceramics for white LEDs. *Journal of Non-Crystalline Solids*, 476, 100-107.

Lyuchao, Z., He, F., Shimin, H., Zhijun, Z., Wang, Y., Rihua, M., Jingtai, Z. (2019). The luminescent properties comparison of RE_2O_3:Eu (RE=Lu,Y,Sc) with high and low Eu doping concentrations. *Journal of Alloys and Compounds*, 781, 302-30.

Matas, J., Paulius, M., Martynas, M., Lina, M., Simas, S. (2016). Luminescence and luminescence quenching of highly efficient $Y_2mo_4o_{15}:Eu^{3+}$ phosphors and ceramics. *Scientific Reports*, 26098, 1-12.

Matas, J., Paulius M., Martynas M., Julija, G., Lina, M. (2016). Luminescence and luminescence quenching of highly efficient $Y_2Mo_4O_{15}:Eu^{3+}$ phosphors and ceramics. *Scientific Reports*, 6, 1-12.

Meng, F. Zhang, J. Zhang, Z. (2015). Luminescence and decay behavior of divalent europium activated barium borophosphate polycrystalline ceramics in the temperature regime 10–525 K. *Ceramics International*, 41,9,11726-11732.

Mengjie, Z., Hongbo, Z., Xiangyu, Z., Wentao, J., Chunhui, S. (2019). Effect of microstructure on up-conversion luminescent of Tb^{3+}/Yb^{3+} co-doped phosphate glass and glass-ceramic. *Materials Letters*, 243, 73-76.

Qiu, J. Cheng, X. Zhang. Y. (2017). Enhanced quantum efficiency with magnesium doping in europium-containing silicon oxynitride phosphor. *Ceramics International*, 43, 17, 14858-14864.

Santos, J. C. A. Silva, E. P., Sampaio D.V., Alves, Rezende, Y. G. S. Kucera, M. V. S. Ballato, C. J. Silva, R.S. (2019). Structural, microstructural, and luminescent properties of laser-sintered Eu-doped YAG ceramics. *Optical Materials*, 89,334-339.

Sen, R., Boetti, N. N. G., Hokka, M., Petit, L. (2019). Optical, structural and luminescence properties of oxyfluoride phosphate glasses and glass-ceramics doped with Yb^{3+}. *Journal of Non-Crystalline Solids*: X, 1, 100003.

Shi, Z. M. Dong, J. H. Ma, W. (2013). Progress in Materials and Processes. Advanced Materials Research, 602-604. 618.

Song, Z., Xu, Y., Li, C., Li, Y., Zhao, Z., Yang, Z., Yin, Z., Li, H. and Qiu, J. (2013). Synthesis and photoluminescence properties of $MgAl(PO_4)O:Eu^{3+}$ red phosphor for white LEDs. *Ceramics International*, 39, 2821-2825.

Wang, H. Yang, Q. Jiang, X. D. Huang. (2017). Optical spectroscopy studies of Ho/Yb co-doped yttrium lanthanum oxide transparent ceramics *Journal of Luminescence*, 192, 752-756.

Wojciech, M., Jadwisienczak, K., Wisniewski M., Spencer G.(2010) Optical properties, luminescence quenching mechanism and radiation hardness of Eu-doped GaN red powder phosphor. *Radiation Measurements*, 45, 500-502.

Xiangyu, L., Guohua, C., Yong, C., Tao, Y. (2017). Luminescent characteristics of $Tm^{3+}/Tb^{3+}/Eu^{3+}$ tri-doped phosphate transparent glass ceramics for white LEDs. *Journal of Non-Crystalline Solids*, 476, 100-107.

Xiaobin, R., Manting, P., Chengguo, M., Aihua, Z., Dandan, J., Feng, S. (2019). Stable temperature characteristic of phosphate glass ceramic for white light-emitting diode. *Micro & Nano Letters*, 14, 113-115.

Xin L., Bowen C., Bingtian T., Hao W., Weimin W. (2017). Variation of structure and photoluminescence properties of Ce^{3+} doped MgAlON transparent ceramics with different doping content. *Materials (Basel)*, 729, 1-10.

Xu, J. Ueda, J. Kuroishi, K. Tanabe, S. (2015). Fabrication of Ce^{3+}-Cr^{3+} co-doped yttrium aluminium gallium garnet transparent ceramic phosphors with super long persistent luminescence. *Scripta Materialia*, 102, 47–50.

Zhi Z., Yi Wang C., Xu Liang L., Pin Z., Guang Zhen C. (2019). Synthetic method for preparing high-performance europium-doped up-conversion ceramic material precursor. *Materials Science Forum*, 953,101-112.